Conduits of steady-state autocatalytic plumes

Michael C. Rogers,[1] Mick D. Mantle,[2] Andrew J. Sederman,[2] and Stephen W. Morris[1]
[1]*Department of Physics, University of Toronto, 60 St. George Street, Toronto, Ontario, Canada M5S 1A7*
[2]*Department of Chemical Engineering, University of Cambridge, Pembroke Street, Cambridge, CB2 3RA, United Kingdom*
(Received 21 September 2007; published 11 February 2008)

Plumes are typically formed when a continuous source of buoyancy is supplied at a localized source. We studied laminar plumes where buoyancy is supplied by an autocatalytic chemical reaction: The iodate-arsenous acid (IAA) reaction. The nonlinear kinetics of the IAA reaction produces a sharp propagating front at which buoyancy is produced by exothermicity and compositional change. When the reaction is initiated in an unconfined volume of reactant, a starting plume with a mushroom shaped head connected to the initiation point by a long conduit is formed. After the initial transient during the ascent of the head, we observed the emergence of a steady state in the conduit morphology and flow. Autocatalytic plumes were compared to nonreacting, compositionally buoyant plumes using the Gradient Echo Rapid Velocity and Acceleration Imaging Sequence (GERVAIS), an MRI velocimetric technique. Autocatalytic conduits had axisymmetric bimodal velocity profiles and cone-shaped morphologies, in contrast to the Gaussian profiles and cylindrical shapes of nonreacting conduits. The bimodal distribution for autocatalytic plumes is a consequence of the unique effect of entrainment in this system. Rather than the usual effect of entrainment in nonreacting plumes, where less buoyant fluid is incorporated into the plumes, entrainment in autocatalytic plumes provides a buoyancy flux along the entire conduit by means of chemical reaction, thereby delocalizing the buoyancy source.

DOI: 10.1103/PhysRevE.77.026105 PACS number(s): 82.40.Ck, 47.20.Bp, 47.70.Fw

From the eruption column of a volcano to the mushroom cloud of an atomic bomb, plumes of rising material form magnificent flow structures [1,2]. A transient plume from a continuous source of buoyancy with a well-defined head is called a *starting* plume. The most visually striking feature of a starting plume is the plume *head*, sometimes called the *cap*, which often takes the form of a vortex ring. However, it is the persistence of the columnar *conduit*, also known as the *stem*, following behind the head that plays a significant role in many geophysical processes. Long-lived plume conduits are believed to underlie the formation of mantle hot spots, such as the one responsible for the Hawaiian Island–Emperor Seamount chain [3]. Entrainment and flow in the conduit is important to the morphology and dynamics of all long-lived plumes. In this study, we used magnetic resonance velocimetry to examine the steady state, laminar plume conduits that emerge from an unconfined autocatalytic chemical reaction [4].

Autocatalytic reactions have highly nonlinear kinetics which, when combined with diffusion, can produce a wide variety of spatially patterned concentration fields which often take the form of propagating fronts or oscillating waves of reaction [5]. In this paper, we consider the iodate-arsenous acid (IAA) reaction [6] in which the diffusion of the autocatalyst ions, iodide and hydrogen, localizes the reaction to a thin propagating front separating reacted and unreacted solutions. It has long been known that such reactions can also produce density changes in the solution, which can couple to fluid flow by causing buoyancy-driven convection [5,7–14]. In the absence of any external forcing, the resulting phenomena are effectively self-stirred reacting flows. The IAA reaction with convection has been compared to a rising astrophysical flame bubble [15].

In the IAA reaction, a small density change across the front is caused by thermal expansion due to the slight exothermicity of the reaction, and also by the solutal density decrease of the product solution [7]. Convection in autocatalytic reactions has generally been studied in confined, one- or two-dimensional geometries [5,7,8,11–14]. In this paper, in contrast, we examine the case of an unconfined, three-dimensional fluid, in which the reaction is free to produce a fully developed starting plume [4]. For simplicity, a plume produced by the IAA reaction will be referred to simply as an autocatalytic plume. We focus on the conduit structure that trails the rising head of the autocatalytic plume, and which persists after the head has reached the top of the reaction vessel. As a control, and for comparison, we also examine nonreacting plume conduits, which were produced by injecting compositionally buoyant fluid into ambient fluid. To probe the internal velocity structure of the plumes, we used a magnetic resonance imaging velocimetric technique known as the Gradient Echo Rapid Velocity and Acceleration Imaging Sequence (GERVAIS) [16]. This technique was used to measure the axial velocity field at various locations along plume conduits.

I. EXPERIMENT

The experimental apparatus consists of a cylindrical glass pipe (the reaction vessel) inserted into the bore of an MRI spectrometer, as shown in Fig. 1. The bottom end of the pipe has a glass floor with a vertical glass capillary tube built into its center. The top end of the pipe was left open. The capillary tube was sealed at the outside (bottom) end with rubber tubing. The pipe used in the experiment is 1.25 m in length, with an inner diameter of 55 mm. The inner diameter of the capillary tube is 3.0 mm. For all experimental runs in which an autocatalytic chemical plume was produced, the glass pipe was filled with 700 mL of reactant solution consisting of $[IO_3^-]=0.005M$, $[As(III)]=0.020M$, $2\times10^{-5}M$ congo red indicator, and 40% glycerol by volume in water. The prepa-

 ©2008 The American Physical Society

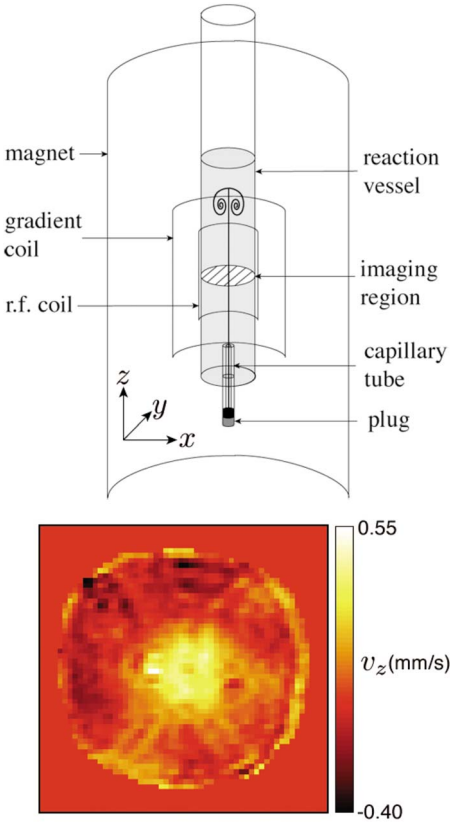

FIG. 1. (Color online) Top: Schematic diagram of the cylindrical reaction vessel placed inside the bore of the MRI spectrometer (shown in cross section). Bottom: Typical MRI velocity image of an autocatalytic chemical plume when the imaging region is 15 cm above the outlet of the capillary tube. The size of the imaging region in view is 64×64 mm, and $v_z = 0$ is indicated by the color of the imaging region surrounding the pipe.

ration of this solution and the measurement of some of its physical properties are described in Ref. [4]. Reactions were initiated by injecting a small amount (less than 0.1 mL) of catalyst solution into the rubber tubing at the bottom end of the capillary tube using a hypodermic syringe. Once initiated, a reaction front would ascend vertically into the capillary tube, where it would proceed upward at a speed of $\sim 1 \times 10^{-3}$ cm/s. Upon reaching the top of the capillary tube, which was immersed in reactant solution, the reaction front continued to move slowly upward. Eventually, the reaction front formed a plume of product solution rising into the ambient reactant solution.

For comparison, nonreacting, compositional plumes were studied in the same glass pipe used for autocatalytic plume experiments. Since compositional plumes must be created by continuous injection of buoyant fluid into the pipe, a syringe pump was connected to the bottom end of the capillary tube, allowing fluid to be injected at a desired rate. The syringe was filled with 38% glycerol solution by volume, and the cylindrical vessel was filled with 40% glycerol solution, giving it the same glycerol-water composition as was used for autocatalytic plume experiments. Using an Anton Paar DMA 5000 density meter, the density of each of these solutions at 20.0 °C were measured to be 1.1160 ± 0.0003 g/cm^3 for the 40% solution and 1.1097 ± 0.0003 g/cm^3 for the 38% solution. Experimental runs were made for injection flow rates from 0.5 mL/min to 2.0 mL/min. All experiments were performed at room temperature, which was approximately 20 °C.

The MRI spectrometer used in our experiments is a Bruker BioSpin DMX 200 with a vertical 149 mm bore 4.7 T superconducting magnet operating at a ^{1}H frequency of 199.7 MHz with a 64 mm birdcage radio frequency probe. A Bruker water-cooled three-axis shielded gradient system used with BAFPA 40 A amplifiers was used to achieve spatial resolution. Magnetic resonance velocity images can be obtained for coherent molecular motion, thus allowing for the determination of a velocity field for a flow. Flow was quantified in our experiment by using phase shift velocity imaging [17]. Velocity images were obtained by utilizing the GERVAIS pulse sequence [16], which is used to calculate velocities from phase shifts in the images produced from a velocity encoding pair of magnetic field gradient pulses. The pulse pair imparts a phase shift that is proportional to the velocity in the direction of the gradient. In our experiments, gradients in the axial z direction, i.e., the direction of plume ascent, were used for encoding the vertical (v_z) motion of fluid passing through a horizontal cross section of the vessel. In different experimental runs, the position of this cross section could be selected to be various distances from the end of the capillary tube, thereby allowing for the examination of conduits at different locations. However, during an experimental run, the location of the horizontal cross section of interest remained stationary. Each image was acquired in 20 ms and images were acquired every 3 s. The field of view was 70 mm $\times$ 70 mm with a slice thickness of 2.5 mm. The velocity encoding was done over a duration of 5.1 ms and the velocity field of view was 13.2 mm/s.

Once the IAA reaction front moves into the reaction vessel, the system enters a period where quiescent fluid is driven into motion by the conversion of reactant to the stable product. During this time, there is an initial transient period of fluid flow followed by a much longer lasting steady state period. During the transient period, initially a slow creeping plume of product solution is formed. From this creeping plume, a starting plume with a well-defined head eventually develops, and later the plume head pinches off from the plume conduit, forming a free vortex ring. The location of pinch off nucleates another plume head, and the process of pinch off is repeated. The evolution of the plume during the transient period is described in detail in Ref. [4]. Once the series of pinch offs stops and the transient period ends, a steady stream of reacted solution forms a conduit that delivers product solution to the top of the vessel. Here, at the top of the vessel, the product solution accumulates, forcing its way downward as its volume increases, eventually engulfing all of the upwelling conduit. Using the apparatus described in [4], digital photographs showing the evolution of an autocatalytic plume and subsequent formation of a long-lived conduit are shown in Fig. 2. If we consider a horizontal cross section of the flow at a given height intermediate to the outlet and the surface of the fluid, we initially see transient behavior when the plume first penetrates the cross section, but soon after the flow of the plume conduit reaches a steady

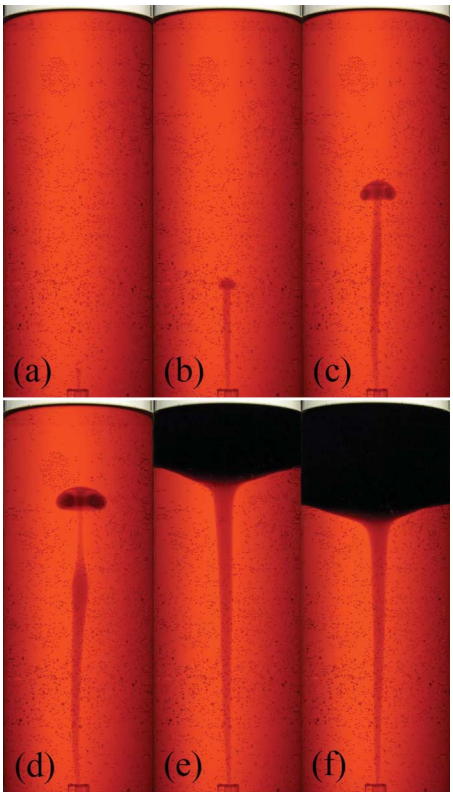

FIG. 2. (Color online) Sequence of images during the evolution of an autocatalytic chemical plume. During the ascent of the plume head toward the top of the container, as shown in (a) through (c), the plume head grows, and in (d) it pinches off, forming a free vortex ring. The point of pinch off proceeds to swell, nucleating a new plume head. As the steady flow of product solution moves upward by means of the conduit, a growing volume of product solution accumulates at the top of the vessel, as shown in (e) and (f). Using $t=0$ as the time at which the front first emerged from the capillary tube, the times at which the pictures were taken in (a) through (f) are $t=67$, 253, 371, 443, 1492, and 2302 s, respectively. The distance from the capillary tube to the top surface of the fluid is 21.6 cm; the inner diameter of the cylinder containing the plume is 8.9 cm.

state. This state was found to persist until the growing volume of product solution made its way downward and moved through the cross section. Here we consider only flow across a given cross section during the time in which the conduit is in steady state flow.

II. RESULTS AND DISCUSSION

Before we consider the detailed structure of the conduit, it is useful to characterize the autocatalytic plume by various dimensionless numbers. This allows us to characterize the concentration, temperature, and flow fields in a general way, and to compare autocatalytic plumes with convection driven chemical fronts in confined geometries.

We then describe the flow profiles we observed, and how the conical shape of the conduit emerges, and how it compares to the conduits found in nonreacting compositional plumes.

A. Dimensionless scaling of the plumes

The Reynolds number achieved by the autocatalytic plumes was

$$\mathrm{Re} = vR/\nu \sim 1, \tag{1}$$

where $R \sim 1$ cm is the diameter of the conduit, $v \sim 0.05$ cm/s is the ascent velocity, and $\nu = 3.81 \times 10^{-2}$ cm^2/s is the measured kinematic viscosity of the solution. While the flow is certainly laminar, it is not so slow as to be considered Stokes or creeping flow, for which $\mathrm{Re} \ll 1$.

The autocatalytic plumes were driven by a combination of thermal expansion due to the heat of reaction and the solutal density decrease of the product solution. Earlier work on convection in autocatalytic fronts in thin vertical tubes and small vertical gaps [9,10] combined these buoyancy effects into a dimensionless density jump $\delta = (\rho_u/\rho_r) - 1$ across the thin front, where ρ_r and ρ_u are the densities of the reacted and unreacted solutions. A dimensionless parameter

$$S = \frac{\delta g a^3}{\nu D} \tag{2}$$

was used to characterize the relative importance of buoyancy in the system. Here g is the acceleration due to gravity, a is either the tube radius or the gap width, ν is the kinematic viscosity, and D is the molecular diffusivity of the autocatalyst. More recently, thermal expansion and solutal density changes have been considered separately in numerical simulations of flow in porous media and Hele-Shaw cells. Following the formulation in Refs. [14,18,19], but replacing the porous medium equations with the full Navier-Stokes equations, two separate Rayleigh numbers may be used to characterize the contribution to buoyancy from the thermal and solutal effects,

$$\mathrm{Ra}_T = \frac{g\alpha L^3}{\nu D}\Delta T \quad \text{and} \quad \mathrm{Ra}_c = \frac{g\beta L^3}{\nu D}\Delta c, \tag{3}$$

where ΔT and Δc are the temperature and concentration differences across the reaction front. Here, α and β are the thermal and compositional expansion coefficients. L is a length scale for which there are several possible choices, as discussed below. Ra_T and Ra_c are the thermal and concentration Rayleigh numbers; replacing a in Eq. (2) with L, the length scale, the sum of Ra_T and Ra_c is equivalent to the driving parameter S, which multiplies the buoyancy driving terms in the Navier-Stokes equations. Ra_T and Ra_c differ from the conventional definition of Rayleigh number,

$$\mathrm{Ra} = \frac{g\alpha L^3}{\nu\kappa}\Delta T, \tag{4}$$

by the replacement of κ, the thermal diffusivity, with D.

Other dimensionless numbers that may be used to characterize autocatalytic chemical plumes are the Schmidt number, $\mathrm{Sc} = \nu/D$, the Lewis number, $\mathrm{Le} = \kappa/D$, and the ratio of Sc and Le, the Prandtl number, $\mathrm{Pr} = \nu/\kappa$. Le is also the factor by which Ra_T is greater than Ra. The glycerol in solution increases ν by about a factor of 4 over that of water, but reduces D. Using the Stokes-Einstein relation [20], we find $D = 4.3 \times 10^{-6}$ cm^2/s. From this, we find $\mathrm{Sc} \approx 9000$ and Le

≈ 280, using $\kappa = 1.2 \times 10^{-3}$ cm^2/s. The large value of Le indicates that heat diffuses much faster than concentration, so we expect the reaction front to be very sharp compared to the smoother temperature field that will surround the plume. Similarly, Pr=32 indicates that the flow field due to the viscous response of the surrounding fluid will be smoother still, compared to the thermal field.

The most natural choice for L is the small length scale ℓ which emerges from the chemical rate constants. The thickness of the reaction front scales with ℓ, which is by far the shortest length scale in the problem. ℓ can be estimated by introducing a reaction time scale $\tau = 1/(\gamma \Delta c^2)$, where γ is a kinetic constant [14,18,19]. Then $\ell = \sqrt{D\tau}$. Using $\gamma = k_b[H^+]^2 = 1800$ M^{-2}s^{-1}, $\tau = 22$ s, $\ell = 1 \times 10^{-2}$ cm, which gives $\mathrm{Ra}_T \approx 1.2$ and $\mathrm{Ra}_c \approx 2.0$ [21,22]. The characteristic velocity, $U = \ell/\tau = 4.5 \times 10^{-3}$ cm/s, is on the order of the velocity measured for traveling fronts in the absence of convection, which were measured to travel downward in a capillary tube at 9.9×10^{-4} cm/s. In this scaling, then, we find that the plumes are rather weakly driven because $\mathrm{Ra}_T + \mathrm{Ra}_c$ is quite small. In the plume configuration, however, there is no threshold, or critical value of the driving parameter below which the front is hydrodynamically stable. In vertical tubes, where the length scale L is taken to be a, the radius of the tube, fronts are stable against convection for $S = \mathrm{Ra}_T + \mathrm{Ra}_c < 87.9$ [10]. In our plume experiment, if L is taken to be the radius of the tube, $\mathrm{Ra}_T + \mathrm{Ra}_c$ becomes very large, of order 10^7. Perhaps the most sensible scale to adopt for comparing plumes to tube and slot experiments is $L \sim R$, the radius of the plume itself. In this scaling, $\mathrm{Ra}_T + \mathrm{Ra}_c \sim 10^6$, still very large.

It should be noted that the above formulation for the reaction time scale is for an IAA system that is buffered to have a constant pH. In our unbuffered system, we make use of the pH change that occurs across the reacting front to visualize the location of the front. However, as shown in Ref. [23], the front propagation velocity changes very little within the pH change that we measure for our reacted and unreacted solutions. The unreacted solution has a pH of ~5.9, while the reacted solution has a pH of ~2.7.

From these scaling considerations, we conclude that the plumes are much more strongly driven by buoyancy than any convecting IAA reaction previously considered, yet they still occur at very moderate Reynolds numbers, and hence should be well described by laminar flow.

B. Velocity profiles of plume conduits

Fluid velocities in the vertical direction were measured across horizontal cross sections of the reaction vessel at distances of 10 cm and 15 cm from the outlet of the capillary tube. A typical MRI velocity image of the vertical velocity profile for the conduit of a plume at 10 cm from the outlet is shown in Fig. 1. Each value, or voxel, in the 64×64 data matrix represents a separate velocity measurement.

Using data obtained during the period of time in which the conduit maintained steady state flow, we radially averaged velocity images to obtain a characteristic velocity profile for a given height above the outlet. This was done by grouping voxels into annuli at various radii from the centroid of the positive components of the velocity distribution. Using the centroid of the plume velocity distribution to define the axis of symmetry of the plume rather than the center of the pipe was necessary to account for the slow drift of the conduit in the x-y plane. This was caused by small drifts in the orientation of the downgoing return flow in the unreacted fluid. Each annulus had a width of 1 voxel, which corresponds to ~1.1 mm, and all velocities found in a given annulus contribute toward the overall average for that annulus. Error bars were calculated from the standard deviations in these values. The velocity values for each annulus were averaged over time (i.e., over several successive velocity images) to obtain the velocity profile as a function of radius from the center of the plume. Using this method, typical velocity profiles obtained for autocatalytic and compositionally buoyant plumes are shown in Fig. 3. For comparison of the velocity profiles with composition profiles, conduits were produced in the apparatus used in Ref. [4] under the same conditions as in the MRI spectrometer, in which the concentration profile was captured with a charge-coupled device (CCD) camera. Since a buffer was not used to control the concentration of hydrogen, congo red indicator could be used to visualize the location of the front of the hydrogen catalyst, which appear as shown in Fig. 2. Along with velocity profiles, Figs. 3(b) and 3(c) show the radius of the reaction front at the respective z position for which the velocities were determined. These radii values were found by averaging the radius at each position for five experimental runs, and were found to be 2.9 ± 0.2 mm at $z = 10$ cm and 3.6 ± 0.1 mm at $z = 15$ cm.

Compositionally buoyant plumes were driven by continuously injecting 38% glycerol solution into 40% glycerol solution, using injection flow rates in the range of 0.5 mL/min to 2.0 mL/min. In this range, the compositionally buoyant plumes were found to have Gaussian velocity distributions where the maximum velocity occurs along the axis of the plume, as shown in Fig. 3(a). As discussed in Ref. [24], such a velocity profile may be phenomenologically described by

$$u_z(z,r) = u_0 e^{-r^2/R^2}, \tag{5}$$

where u_0 is the maximum z component of the velocity above the origin at $z=0$, r is the distance from the axis of symmetry of the plume, and R is the radial length scale of the velocity distribution. By use of shadowgraphy, we also determined the edge of the concentration profile of the compositional plumes, which remains quite sharp compared to the velocity profile because of the large Schmidt number. In both compositional and autocatalytic plumes, the velocity profiles extend well beyond the plume edge because of the laminar shear created by the viscous entrainment between rising plume material and ambient fluid. Since the tube diameter is not infinite, continuity requires a $u_z < 0$ return flow, which the MRI velocimetry identifies near the outer edge of the tube. Only velocity values above zero were used in the Gaussian fits shown in Fig. 3.

For the compositional plumes, the velocity profile length scale R remained independent of z, and the plume conduit maintained its cylindrical shape. Consistent with this, the

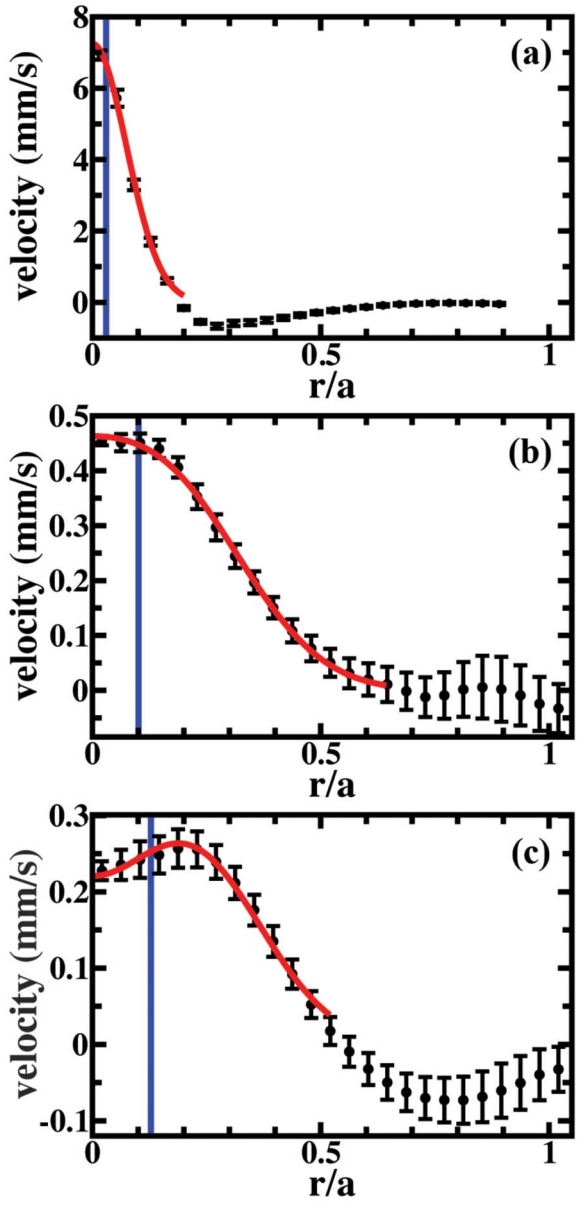

FIG. 3. (Color online) Averaged axial velocity profiles derived from MRI velocity images for (a) a compositionally buoyant plume 10 cm from the capillary tube outlet produced by an injection flow rate of 2.0 mL/min, and an autocatalytic plume (b) 10 cm from the outlet and (c) 15 cm from the outlet. r indicates the distance from the plume axis, and a is the radius of the glass tube. Vertical lines represent the location of the reaction front, or plume edge. The curve in (a) shows a Gaussian fit of the velocity data, and the curves in (b) and (c) show axisymmetric bimodal Gaussian fits. Gaussian fits were performed only for positive velocity values. Negative velocities are due to the broad downward return flow generated by the plume. The number of consecutive velocity images averaged for each profile were (a) 36, (b) 91, and (c) 128, where each velocity image was 3 s apart.

diameter of the concentration profile also remained constant. In such a plume, one would expect essentially no entrainment of the surrounding fluid into the plume by means of molecular diffusion or viscous stresses.

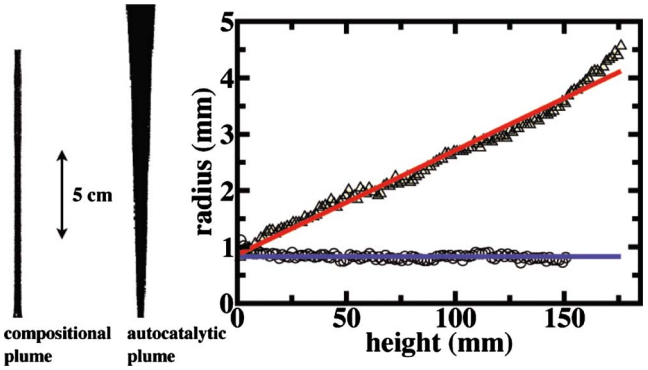

FIG. 4. (Color online) Left: Typical morphology of a compositional and an autocatalytic plume, obtained from image analysis of experimental data, shown to scale. Right: Radius of the autocatalytic plume (△) and compositional plume (○), and their lines of best fit, as a function of height from the capillary tube outlet.

These simple features are different in autocatalytic conduits. Figure 3(b) shows the velocity profile for an autocatalytic conduit at $z=10$ cm from the capillary tube outlet. Here, velocities measured across the radius of the conduit remain almost as high as they do along the plume axis, significantly flattening its velocity profile. Farther up the pipe, at $z=15$ cm, the velocity profile within the plume is no longer maximum near the conduit centerline, as shown in Fig. 3(c). The velocity maximum is localized in the vicinity of the reacting front.

These new features are due to the continuous flux of buoyancy occurring along the entire length of the conduit. The buoyancy flux comes from both the production of heat occurring at the reaction front located at the composition edge, and from the radial entrainment of reactant solution into the plume. This inward flux of reactant, which becomes

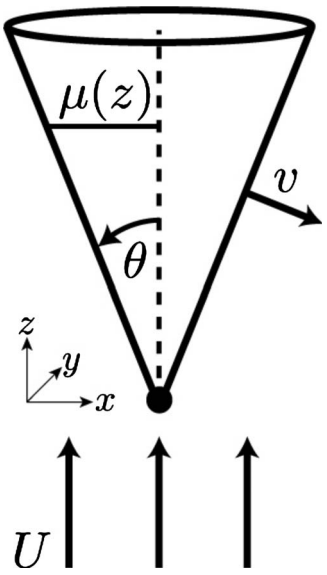

FIG. 5. Simple geometrical model of an autocatalytic plume conduit. The cone half-angle is θ; the radius of the cone as a function of distance above $z=0$ is $\mu(z)$.

product as it crosses the sharp reaction front, also creates a buoyancy flux due to its solutal composition change. This flux of buoyancy into an autocatalytic plume is in stark contrast to the role of entrainment of outer fluid into nonreacting plumes, where entrainment modifies the behavior of plumes by enlarging them by incorporating denser fluid into their structure [25]. The advance of the front combines with the upward fluid velocity to cause the conduit diameter to increase with z, giving the concentration profile a conical shape, as shown in Figs. 2(e) and 2(f). This is in contrast to the constant diameter conduits that were observed for nonreacting, compositional plumes. When the diameter of the conduit is sufficiently large, the upward flow within the plume is fastest at its edge, and a minimum appears in the velocity profile along the axis.

The velocity profile of the more complex autocatalytic conduit can be phenomenologically described by a symmetric bimodal distribution of the form

$$u(z,r) = u_0[e^{-[r-\mu(z)]^2/\sigma^2} + e^{-[r+\mu(z)]^2/\sigma^2}], \tag{6}$$

where $\mu(z)$ is the radial distance between the axis of symmetry and the sharp chemical front. Clearly, the width σ of the maximum localized near the front must be related to the length scale over which the heat of the reaction is diffused, creating part of the buoyancy that drives the flow. As the conduit radius $\mu(z)$ becomes larger, it eventually exceeds this length, and the velocity minimum on the axis becomes apparent. The bimodal shape is a good phenomenological description of the velocity field of an autocatalytic plume because these plumes do not have a localized source of buoyancy. Rather, they have a distributed "sheet" source of buoyancy that exists all over the surface of contact between reacted and unreacted species. The entire conduit edge is a conical reaction front that provides buoyancy to the plume.

C. Conical shape of the concentration front

In separate indicator and shadowgraph experiments, for autocatalytic and compositional plumes, respectively, the radii of the edge of the steady state plume conduits, such as the autocatalytic conduits shown in Figs. 2(e) and 2(f), were determined as a function of z using image analysis. Figure 4 shows a comparison. The autocatalytic conduit achieves a steady, approximately conical shape, characterized by a half-angle $\theta \approx 1.7°$, as determined by averaging the conical spreading of several plumes. The compositional conduit remains cylindrical.

The autocatalytic conduit attains a remarkable steady state, which is a balance between upward flow, buoyancy production, and the advance of the chemical front due to diffusion of the autocatalyst. The spreading of the conical conduit is sufficient to balance the front speed v and the upward hydrodynamic flow U, as shown in Fig. 5. For our reactant composition, the measured front speed in the absence of convection is $v = 9.9 \times 10^{-3}$ mm/s [26]. At this front speed, a half-angle of 1.7° should be achieved for $U = v/\sin\theta \sim 0.3$ mm/s. Typical upward velocities of fluid in an autocatalytic plume, as measured by MRI velocimetry, lie in the range of $\sim 0.2-0.5$ mm/s, in agreement with this simple picture.

III. CONCLUSIONS

We have described a study of the steady state plume conduits produced by the IAA reaction. We have quantified the flow profile and morphology of these conduits, and compared them to plume conduits produced by nonreacting glycerol-water mixtures. To examine the flow profile we used a dynamic MRI imaging sequence called GERVAIS to resolve vertical velocity components across a horizontal cross-section of the pipe housing the rising plume. We found that the vertical flow across a chemical plume conduit may be phenomenologically described by an axisymmetric bimodal distribution, one that widens in accordance with the approximately uniform conical widening of the plume. This is in contrast to the Gaussian velocity distribution that describes flow across a nonreacting plume conduit that remains cylindrical. This finding shows that the buoyancy flux that drives the plume upward is created by the plume boundary, or reaction front. Such an addition of buoyancy by means of entrainment is unique to IAA chemical plumes, since entrainment of ambient fluid in a nonreacting system incorporates less buoyant fluid into the plume. This creates a unique scenario whereby the source of buoyancy for an autocatalytic plume is distributed along the entire plume boundary, instead of the buoyancy being supplied solely at a localized source as is the case for nonreacting plumes.

ACKNOWLEDGMENTS

M.C.R. acknowledges support from the Department of Applied Mathematics and Theoretical Physics at the University of Cambridge. We thank Anne De Wit and Abdel Zebib for valuable discussions. M.D.M. and A.J.S. acknowledge financial support through Grant No. GR/S20789/01 and the EPSRC for the provision and L. F. Gladden for the use of the NMR spectrometer. This research was also supported by the Natural Science and Engineering Research Council (NSERC) of Canada.

[1] P. Francis and C. Oppenheimer, *Volcanoes*, 2nd ed., (Oxford University Press, Oxford, 2004).
[2] S. R. Weart, *Nuclear Fear: A History of Images* (Harvard University Press, Cambridge, MA, 1998).
[3] W. J. Morgan, Nature (London) **230**, 42 (1971).
[4] M. C. Rogers and S. W. Morris, Phys. Rev. Lett. **95**, 024505 (2005).
[5] I. R. Epstein and J. A. Pojman, *An Introduction to Nonlinear Chemical Dynamics* (Oxford University Press, Oxford, 1998).
[6] A. Hanna, A. Saul, and K. Showalter, J. Am. Chem. Soc. **104**, 3838 (1982).
[7] J. A. Pojman and I. R. Epstein, J. Phys. Chem. **94**, 4966

(1990).
[8] J. A. Pojman, I. R. Epstein, T. J. McManus, and K. Showalter, J. Phys. Chem. **95**, 1299 (1991).
[9] D. A. Vasquez, B. F. Edwards, and J. W. Wilder, Phys. Rev. A **43**, 6694 (1991).
[10] D. A. Vasquez, J. W. Wilder, and B. F. Edwards, Phys. Fluids A **4**, 2410 (1992).
[11] M. R. Carey, S. W. Morris, and P. Kolodner, Phys. Rev. E **53**, 6012 (1996).
[12] M. Bockmann and S. C. Müller, Phys. Rev. Lett. **85**, 2506 (2000).
[13] A. De Wit, Phys. Rev. Lett. **87**, 054502 (2001).
[14] J. D'Hernoncourt, A. De Wit, and A. Zebib, J. Fluid Mech. **576**, 445 (2007).
[15] N. Vladimirova, Combust. Theory Modell. **11**, 377 (2007).
[16] A. J. Sederman, M. D. Mantle, C. Buckley, and L. F. Gladden, J. Magn. Reson. **166**, 182 (2004).
[17] M. D. Mantle and A. J. Sederman, Prog. Nucl. Magn. Reson. Spectrosc. **43**, 3 (2003).
[18] A. Zebib and A. De Wit (private communication).
[19] J. D'Hernoncourt, A. Zebib, and A. De Wit, Phys. Rev. Lett. **96**, 154501 (2006).
[20] A. Einstein, Ann. Phys. **17**, 549 (1905).
[21] The following parameter values were used for calculations: $g=981\ \mathrm{cm/s^2}$, $\Delta T=0.5\ ^\circ\mathrm{C}$, $\nu=3.81\times10^{-2}\ \mathrm{cm^2/s}$, $\alpha=4.3\times10^{-4}\ ^\circ\mathrm{C^{-1}}$, $k_b=4.5\times10^8\ \mathrm{M^{-4}s^{-1}}$, $\Delta c=[\mathrm{IO_3^-}]_0=0.005M$, and $[\mathrm{H^+}]=0.002M$.
[22] $\beta\Delta c$ was found by measuring ρ_u and ρ_r in a U-tube densitometer. It was found that $\rho_r=1.1124\ \mathrm{g/cm^3}$ and the isothermal density difference was found to be $\rho_r-\rho_u=4\times10^{-4}\ \mathrm{g/cm^3}$. This gives a solutal dimensionless density jump of $\beta\Delta c=(\rho_u/\rho_r)-1=3.6\times10^{-4}$.
[23] J. Harrison and K. Showalter, J. Phys. Chem. **90**, 225 (1986).
[24] J. S. Turner, J. Fluid Mech. **13**, 356 (1962).
[25] R. W. Griffiths, Phys. Fluids A **3**, 1233 (1991).
[26] Front speed in the absence of convection was determined by measuring a flat descending front in a vertical capillary tube. The inner bore of the tube was 3.0 mm and it was placed inside a fluid jacket held at a constant temperature of 25.0 °C.